RSC Advances

ROYAL SOCIETY OF CHEMISTRY

www.rsc.org/advances

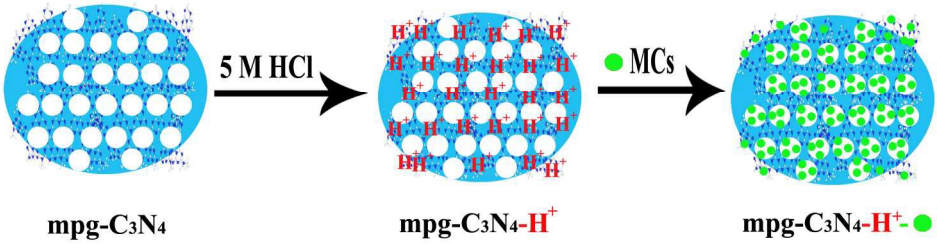

182x68mm (300 x 300 DPI)

Protonated mesoporous graphitic carbon nitride for rapid and high efficient removal of microcystins †

Chuanhui Huang[a], Wenmin Zhang[a], Zhiming Yan[a], Jia Gao[a], Wei Liu[a,b], Ping Tong[a,b]*, Lan Zhang[a,b]*

Received (in XXX, XXX) Xth XXXXXXXXX 200X, Accepted Xth XXXXXXXXX 200X
First published on the web Xth XXXXXXXXX 200X
DOI: 10.1039/b000000x

Cyanotoxins have caused worldwide concerns for their eclectic occurrence and toxic effects, which led to an intensive search of cost-effective techniques for their removal from contaminated waters. In this study, a novel biomaterial protonated mesoporous graphitic carbon nitride (mpg-C_3N_4-H^+) which is fabricated by treat mpg-C_3N_4 with concentrated hydrochloric acid, is applied as a promising bioadsorbent for the uptake of microcystins （MCs）. The pH of the reaction media played a significant role in removal of MCs; maximum adsorption occurred at pH 7. Kinetic studies showed that the adsorption of MC-LR and MC-RR onto adsorbent were a rapid process. The mpg-C_3N_4-H^+ exhibited high adsorption capacity of 2360.96 and 2868.78 μg/g from the Langmuir model for MC-LR/RR, respectively. The high adsorption capacity, good solvent stability, and excellent reusability make mpg-C_3N_4-H^+ promising as a novel adsorbent for the adsorption and removal of MCs from aqueous solution. This information may be useful for further research and practical applications of the novel two dimensional layered, mesoporous graphitic carbon nitride.

1. Introducation

The In the past few years, great efforts have been made to study two dimensional (2D) layered nanomaterials which are one kind of the most fascinating materials for their high specific surface area and distinct properties.[1, 2] As an emerging 2D layered nanomaterials, graphitic-phase carbon nitride (g-C_3N_4) has attracted a great deal of scientific interest because theoretical investigations revealed outstanding mechanical, thermal, unique electronic and optical properties of g-C_3N_4.[3, 4] The g-C_3N_4 contains planar layers with π electron conjugation and is mainly composed of carbon and nitrogen with weak van der Waals force between C−N layers.[5] Since g-C_3N_4 is a chemically and thermally stable semiconductor with a band gap of about 2.7 eV, it has been applied in the fields of catalysis,[6] degradation,[7] sensing,[8] drug delivery[9] and imaging.[10] Very recently, mesoporous graphitic carbon nitride (mpg-C_3N_4) is prepared by soft chemical routes and methods.[11] As a novel kind of g-C_3N_4, mpg-C_3N_4 has a much higher surface area (~200 m^2/g) than the bulk g-C_3N_4 and is valuable for extensively studied.[12, 13] However, finer details of local structure and composition of mpg-C_3N_4 are lacking in many cases, which results also in limitations and uncertainties in potential applications. To solve these problems, postfunctionalization would be a suitable method to raise the properties of mpg-C_3N_4. Among others, direct protonation of base functionalities is a convenient modification route. This follows direct protonation had been used to disperse and process CNTs.[14] Zhang et al. have reported that carbon nitrides can be reversibly protonated by strong mineral acids, thus modifying solubility/dispersability and surface area.[15] Nevertheless, to the best of our knowledge, direct protonate mpg-C_3N_4 and apply the protonated mpg-C_3N_4 as a bioadsorbent has not been explored until now.

Microcystins (MCs) are known for their rapid activity and acute lethal toxicity which can cause damage to livers even at very low concentrations and induce tumour promoting activity through the inhibition of protein phosphatases.[16] To date, over 80 variants of MCs have been discovered. Among them, microcystin-LR (MC-LR) and microcystin-RR (MC-RR) are the most commonly studied MCs. Moreover, a provisional safety guideline of 1.0 μg/L MC-LR in drinking water has been recommended by World Health Organization.[17] Therefore, it is of urgent need to develop a reliable method for rapid and effective removal of MCs from water sources.

To date, various methods have been developed to remove MCs from aqueous solution, such as traditional water treatment technology,[18] chemical oxidation processes,[19] biological methods.[20] However, the above-mentioned methods usually require high dosage, time consuming, may generate toxic disinfection by-products and are thus not viable. More recently, a number of reports have been published on adsorption which is regarded as a simple, effective and time-saving technology for the removal of MCs. Materials including activated carbons (ACs),[21] clays,[22] peats[23] and carbon nanotubes[24] have been explored as potential bioadsorbent in the adsorption process and achieved some success. Pavagadhi et al have examined the ability of graphene oxide to remove both MC-LR and MC-RR from water.[25] Ordered mesoporous silica[26] and mesoporous carbons[27] were also employed for removal of MCs, the results show that mesoporous materials have great potential for uptake of MCs. Xia et al fabricated metal–organic framework MIL-100 (Al) gels for the adsorption of MC-LR.[28] Even so, materials available for high efficient removal of MCs are still quite limited. Thus, it is still of great significance to discover new materials for highly efficient removal of MCs.

Herein, for the first time, we reported a novel bioadsorbent, which was prepared by post modified mpg-C_3N_4 via direct protonation, for rapid and high efficient removal of MCs (MC-LR and MC-RR, the chemical structures of two MCs were shown in (Supplementary data Fig. S1). We found that the protonation process could not only enhance the adsorption capacities for MCs

a Ministry of Education Key Laboratory of Analysis and Detection for Food Safety, Fujian Provincial Key Laboratory of Analysis and Detection Technology for Food Safety, College of Chemistry, Fuzhou University, Fuzhou, Fujian, 350116, China
b Testing Center, The Sport Science Research Center, Fuzhou University, Fuzhou, Fujian, 350002, China, Fax: +86-591-87800172
E-mail: zlan@fzu.edu.cn (L. Zhang), tping@fzu.edu.cn (P. Tong);
† Electronic Supplementary Information (ESI) available: Experimental details and additional figures. See DOI: 10.1039/c0xx00000x

but also greatly accelerate the removal rate. Moreover, the mpg-C_3N_4-H^+ shows much higher adsorption capacities than commercial activated carbon in removing MCs. Adsorption kinetics and isotherms were studied, and the experiments results showed that pseudo-second-order kinetic model and Langmuir isotherm were better fitted for the adsorption of MCs onto bioadsorbent. the thermodynamic parameters, negative free energy change and negative enthalpy indicating that the adsorption is spontaneous, favorable and exothermic reaction in nature. The result strongly exhibits that mpg-C_3N_4-H^+ can be successfully applied to convenient, high efficient and fast removal of MCs dissolved in water.

2. Experimental

2.1. Chemicals and reagents

Commercial colloidal silica (Ludox HS40) is purchased from Sigma–Aldrich (St. Louis, Missouri, USA). MC-LR and MC-RR (>95% purity, HPLC) were obtained from Alexis Biochemicals (Switzerland). All reagents were either HPLC grade or analytical grade. Acetonitrile and formic acid were purchased from Fluka. Methanol is obtained from Sigma–Aldrich at HPLC grade. The MC-LR and MC-RR stock solution is prepared at the concentration of 100 mg/L in methanol. Deionized water (18.2 MΩ) is prepared with a Milli-Q water purification system (Millipore, USA).

2.2. Apparatus

Scanning electron microscopy (SEM) images were obtained with an FEI Inspect F50 (FEI, USA). Transmission electron microscopy (TEM) analyses were performed on a FEI Tecnai G2 F20 (FEI, USA) at 200 kV. Fourier transform infrared (FT-IR) spectra were conducted with a FT-IR spectrophotometer (Nicolet 6700, Waltham, MA, USA). The surface area and pore diameter were determined with a physisorption analyzer (Micromeritics ASAP 2020 porosimeter, USA) at −196 ºC. Before the measurements, samples were degassed in vacuo at 200 ºC for at least 480 min. Brunner−Emmet−Teller (BET) method is used to calculate the specic surface areas (SBET) using adsorption data at p/p_0 of 0.05–0.3. The pore size distributions (PSDs) were derived from the adsorption branches of isotherms by using the BJH model. The total pore volume (Vt) is estimated from the adsorbed amount at p/p0 of 0.995. The X-ray powder diffraction (XRD) pattern is determined using a D8 Advance (Bruker, German). Zeta potentials of the adsorbent in ultrapure water were measured on a zeta potential analyzer (Mastersizer 3000, Marlven). Elemental analysis is performed with a varioMICRO cube form Elementar Analysen systeme GmbH.

2.3. Preparation of the mpg-C_3N_4

The mpg-C_3N_4 is prepared according to the previously reported method.[13] Briefly, 5.0 g of cyanamide is dissolved in a 40% dispersion of 12 nm SiO_2 particles in 12.5 g of water with stirring at 333 K overnight. Then the resulting transparent mixtures were then heated for 4 h to 550 ºC and keep at this temperature for another 4 h in air. The resulting brown-yellow powder is treated with 4 M ammonium bifluoride for 2 days to remove the silica template. The powders were then filtered and washed with distilled water at least 6 times. Afterwards, the powders were stirred in 0.01 M potassium hydroxide solution for another 2 days. Finally the powders were again filtered and washed at least 3 times with deionized water and 2 times with ethanol. The final product is obtained by drying over night at 100ºC under vacuum.

Protonation of mpg-C_3N_4: 1.0 g of mpg-C_3N_4 is mixed with 10.0 mL hydrochloric acid with the concentration of 5.0 M. The solution is kept stirring overnight, followed by filtration and washed with deionized water until neutral condition and drying over night at 100ºC under vacuum.

Preparation of bulk g-C_3N_4: The bulk g-C_3N_4 is prepared by polymerization of dicyandiamide molecules under high temperature. In detail, dicyandiamide is heated at 823 K for 4 h under air condition with a ramp rate of about 2.3 K/min for both of the heating and cooling processes. The obtained yellow product is the g-C_3N_4 powder.

2.4. Batch adsorption experiments

Batch adsorption experiments were conducted to assess the adsorption rate and determine the adsorption equilibrium time. To initiate the experiments, 0.5 mg of mpg-C_3N_4-H^+ is added into a 10.0 mL vial equipped with Teflon-lined screw cap, then 5.0 mL of 50.0 μg/L, 100.0 μg/L, 200.0 μg/L MC-LR and MC-RR solution were added separately, followed the mixture is agitated at 200 rpm, 30ºC in a thermo stated rotary shaker (MRC TU400) for 400 min. At each predetermined time point, 1.0 mL of the mixture is taken out, the solutions were separated from the adsorbent by centrifugation at 8000 rpm for 5 min, then the supernatant is filtered through syringe filters (cellulose acetate membranes) with the size of 0.22 μm to remove the particles after the centrifugation, and each residual concentration of MCs is measured. Control experiments were performed with blanks containing no MB under the same conditions as for the MB solution. Each data point was run in triplicate.

Similarly, adsorption isotherm experiments were conducted to evaluate the maximum adsorption value and the adsorption thermodynamic properties. 0.5 mg of adsorbent is dispersed in 5.0 mL solution with various initial concentrations of MC-LR and MC-RR (20.0–300.0 μg/L), agitating for 180 min in a rotary shaker to reach apparent adsorption equilibrium at different temperatures (20–50 ºC). Control experiments were preformed with 20.0–300.0 μg/L of MCs devoid of adsorbent under the same conditions as adsorption. Each data point is run in triplicate. No noticeable reduction in the initial concentration of MCs studied is observed in controlled experiments.

The pH value of MC solutions is adjusted by using either a 1.0 M formic acid or a 1.0 M ammonium hydroxide solution to different pH (2.0 to 9.0). The effect of ionic strength on MCs adsorption to adsorbent is carried out with background electrolyte (ammonium acetate) concentrations ranging from 0.02 M to 0.1 M. The conditions of the pH dependent adsorption tests and ionic strength dependent adsorption experiments were the same as the batch adsorption above.

2.5. Analytical methods

The concentration of MCs were accurately determined on a LC-MS-MS system which consisted of an Accela HPLC system (Thermo Fisher Scientific, USA) with a vacuum degasser, quaternary pump, autosampler and thermostated column compartment, coupled to a TSQ Quantum Access MaxTM triple quadrupole mass spectrometer (Thermo Fisher Scientific, USA). The analytical separation of the analytes is achieved on a Hypersil GOLD C18 column (5 μm particle size, 150×2.1 mm). The mobile phase is a mixture of acetonitrile (solvent B) and water (45:55) containing 0.1 % of formic acid (v/v). The flow rate is set at 0.2 mL/min. The sample injection volume is 10 μL. An isocratic elution is used with acetonitrile: water at 45:55 at the rate of 200 μL/min.The capillary temperature and vaporizer were set at 350 ºC and 300 ºC, respectively. Sheath gas pressure and auxiliary gas pressure were carried out at 35 bar and 10 bar

separately. The instrument is operated in the positive ion mode. MC-LR and MC-RR were monitored by using the instrument in the SRM mode (m/z 498.5, fragment ion 135.11; m/z 520.0, fragment ion 135.01, respectively).

3. Results and discussion

3.1. Characterization

To investigate the basic composition of the mpg-C_3N_4, XRD is first conducted. The presence of g-C_3N_4 domains is verified by two signals present on the XRD pattern (Fig.1), namely the strong shoulder peak at 2θ of 27.4° (d=0.326 nm), which originates from the (002) interlayer diffraction of a CN graphitic-like structure, and the low-angle diffraction peak at 2θ of 13.3° (d=0.663 nm), which is derived from inplanar repeated tri-s-triazine units. The graphite-like structure of mpg-C_3N_4 is retained after the protonation

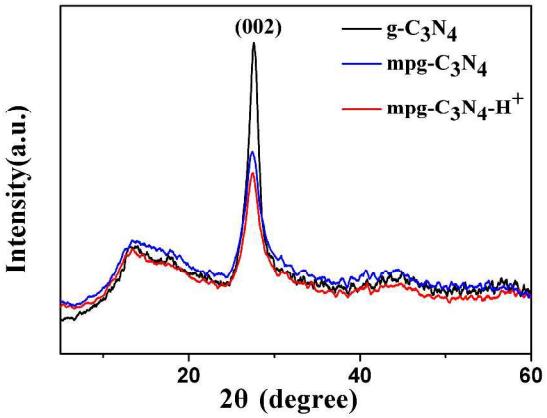

Fig.1. XRD patterns.

In the FT-IR spectrum (Supplementary data Fig. S2a), the peaks at 1637 cm^{-1} and 1243 cm^{-1} were attributable to the C=N and C–N stretching vibration modes, respectively.[29] The peak at 808 cm^{-1} is related to the s-triazine ring modes.[30] After post-functioned with strong acids, no peaks corresponding to an -amide or -OH group which could be related to broken fragments were found as precious report[15], for example, it could be seen apparently that the peak at 1541 cm^{-1} disappeared in mpg-C_3N_4-H^+ (Supplementary data Fig. S2b). It can also be clearly seen that the main characteristic peaks of the mpg-C_3N_4 appear in the mpg-C_3N_4-H^+ which further confirms that the core chemical skeleton of mpg-C_3N_4 has remained unchanged after proton treatment using concentrated hydrochloric acid.

Direct evidence of the protonation came from the increased hydrogen content of protonated mpg-C_3N_4, as determined by elemental analysis. A small amount of hydrogen (ca. 2.0%) is most often observed in the staring mpg-C_3N_4 (more appropriately as mpg-$C_3N_{4.2}H_{2.0}$), which could be due to absorbed water and imperfection of the thermolysis. After the protonation, the hydrogen content of protonated mpg-C_3N_4 increases to 2.7% (more appropriately as mpg-$C_3N_{4.2}H_{2.7}$).

The structure and morphologies of the materials were revealed by FESEM and TEM images (Fig. 2). SEM images reveal the typical slate-like, stacked lamellar texture of milled g-C_3N_4, where the lamellar character is indicated by its preferential cleavage planes. Apparently, the protonation turned grey mpg-C_3N_4 (Fig. 2a) into practically white mpg-C_3N_4-H^+ (Fig. 2b) and the surface quality of the composites is improved evidently. TEM images indicate that a lot of optical spot exist in the material which can be attributed to the empty obtained after

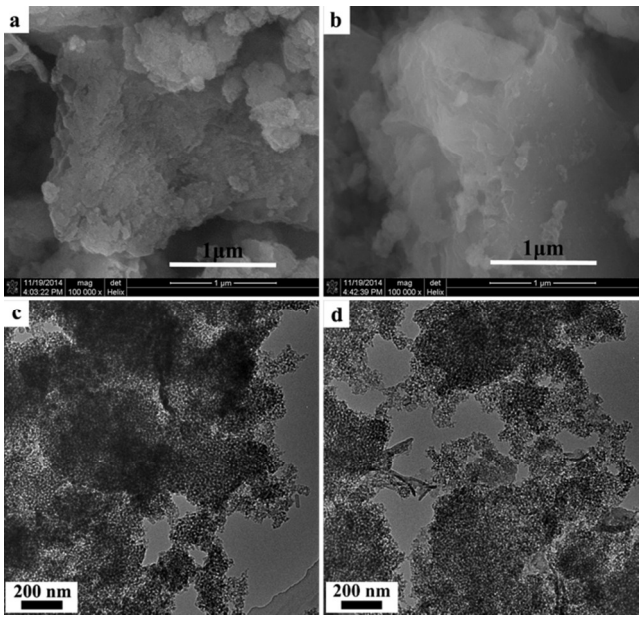

Fig.2. (a) SEM images for mpg-C_3N_4; (b) SEM images for mpg-C_3N_4-H^+; (c) TEM images for mpg-C_3N_4; (d) TEM images for mpg-C_3N_4-H^+.

etching with ammonium bifluoride (Fig. 2c , d). The zeta-potential of mpg-C_3N_4-H^+ dispersions in water is shifted after contact with concentrated hydrochloric acid from negative to positive surface charges almost at every pH value as shown in Fig. S4, which also demonstrates successful protonation.

The N_2 adsorption isotherm measured for g-C_3N_4, mpg-C_3N_4 and mpg-C_3N_4-H^+ resembles type IV with an H3-type hysteresis loop (Fig. 3), which confirms the presence of interconnected mesopores. The mpg-C_3N_4 shows much higher BET surface area than g-C_3N_4. Correspondingly, similar distribution curves were observed on the pore-size for mpg-C_3N_4 and mpg-C_3N_4-H^+. In addition, after the protonation, mpg-C_3N_4-H^+ exhibits a slightly larger total adsorption average pore width, total pore volume, and the experimental multipoint BET surface area of 14.68 nm, 0.71 cm^3, 193.52 m^2/g than mpg-C_3N_4 of 13.65 nm, 0.65 cm^3, 189.78 m^2/g, respectively.

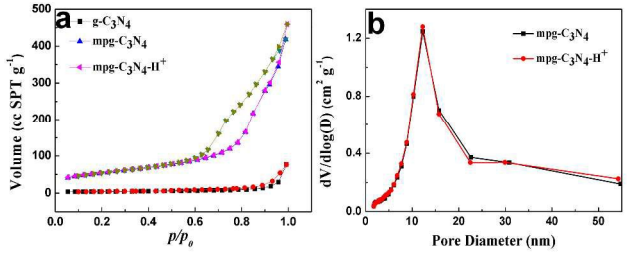

Fig.3. (a) N_2 adsorption–desorption isotherms; (b) Pore diameter distribution profiles.

3.2. Effect of different factors on adsorption

Effect of initial solution pH

The experiments were carried out in pH range 2.0 – 9.0 to examine the effect of pH on the adsorption of MC-LR/RR by mpg-C_3N_4-H^+, the results were illustrated in Fig. 4a. The result showed that the adsorption of MC-LR and MC-RR followed the same trend, the adsorption capacity of mpg-C_3N_4-H^+ for MCs increased as the pH increased from 2.0 to 7.0, then decreased with further increase of pH from 7.0 to 9.0. Therefore, it is clear

that the maximum adsorption is observed at pH 7.0. Therefore, all other experiments were carried out at pH 7.0.

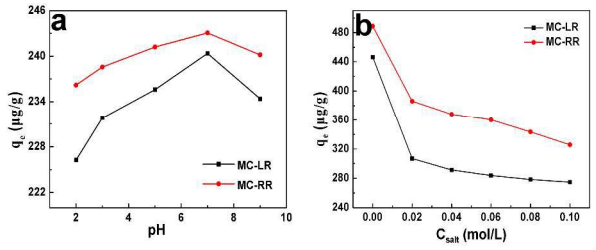

Fig. 4 (a) Effect of pH for the adsorption of MCs (25.0 μg/L) on mpg-C_3N_4-H^+ (0.1 mg); (b) Effect of the concentration of ammonium acetate for the adsorption of MCs (50.0 μg/L) on mpg-C_3N_4-H^+ at 30 °C; pH 7.0.

Since the structure of MCs contains numerous ionizable groups, the overall charge on the toxin is pH dependent. Maagd et al. demonstrated that the MC-LR species remain neutral at the narrow pH range of 2.09 - 2.19; MC-LR is protonated to cationic species [$(COOH)_2(NH_2^+)$] when the pH < 2.09 and deprotonated to anionic species, [$(COO^-)_2(NH)$] and [$(COO^-)_2(NH_2^+)$] at pH > 2.19.[31] Therefore, since MC-RR and MC-LR share similar structures, it can be inferred that they would behave in a similar way. As the solution pH increased from 2.0 to 9.0, the positive charges on the surface of mpg-C_3N_4-H^+ decreased, i.e. less positive zeta potential (Supplementary data Fig. S4), which would have an reduced effect on the adsorption of negatively charged MCs due to electrostatic attraction. Whereas, as the solution pH increased from 2.0 to 9.0, more and more MCs were deprotonated to form COO^- group with negative charge, thereby enhancing the electrostatic attraction between negatively charged MC anions and positively charged surface of mpg-C_3N_4-H^+. The above two opposite effect factors led to the optimal pH at 7.0.

Furthermore, the partitioning effect of charged MC-LR and MC-RR was employed in the present study to explain the decreased adsorption of MC-LR at pH > 7.0. Partitioning is the measure of differential solubility of a compound between two immiscible solvents at equilibrium. Normally, one of the solvents is water and the second one is hydrophobic or nonpolar solvent such as octanol. It correlates with the tendency of a molecule to concentrate in the lipids of organisms and the organic carbon of sediments and soils. As the pH increase from 1 to 10, the n-octanol/water distribution ratio D_{ow} for MC-LR decreases from 2.18 to 1.76, revealing that MC-LR exhibits increased hydrophilicity and consequent decreased partitioning in octanol with the increase in pH. Therefore, with the increase in pH, MC-LR has a tendency to remain in the aqueous phase rather than getting adsorbed. It could be inferred that MC-RR would show very similar kind of response as MC-LR in terms of partitioning due to the similarities in structure between them.

Effect of ionic strength

Generally, there are various salts and metal ions in the natural water. In order to investigate the effect of coexisting ions on adsorption properties of mpg-C_3N_4-H^+, different concentrations of ammonium acetate were added into the adsorption system. As seen in (Fig. 4b), MCs uptake capacities decreased significantly once 0.01 mol/L ammonium acetate is added, furthermore, the MCs removal efficiency dropped persistently with more and more electrolyte exist in the solution. The above results indicate that electrostatic interaction is one of the mechanisms for the adsorption of MCs on adsorbent.

As the result showed in (Fig. 4), the mpg-C_3N_4-H^+ has better adsorption capacity of MC-RR than MC-LR, which is in agreement with that reported previously.[32] It may be attributed to their different molecular compositions. It has been generally accepted that the difference in adsorption capacity mainly comes from the arginine unit instead of leucine at the second position in MC-RR. Hence, there is an increased tendency to form cation bridging and more hydrogen bonds between the adsorbents and MC-RR.[32]

Comparison of the adsorption capacity

In order to further study the mechanisms of adsorption of MCs on mpg-C_3N_4-H^+. The adsorbed quantity of MCs by three adsorbents is compared in (Fig. 5). It shows that mpg-C_3N_4-H^+ has better MCs removal efficiency than mpg-C_3N_4 at different times and the adsorption capacity of mpg-C_3N_4 is much better than that of g-C_3N_4. The uptake efficiency of mpg-C_3N_4-H^+ can be as high as 96% for both MC-RR and MC-LR after contact for 15 min at present concentration. It is clear that the protonation not only enhances the ability of adsorption for MCs but also greatly accelerates the removal rate of MCs.

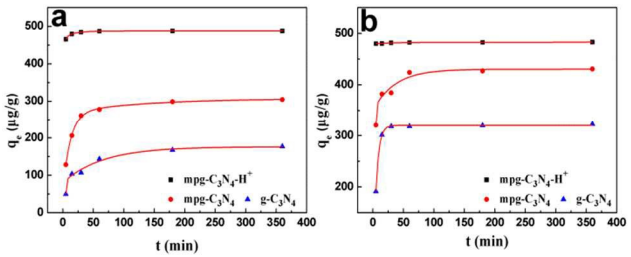

Fig. 5 Adsorption isotherms of MCs (50.0 μg/L) over the three adsorbents at 30 °C; pH 7.0.

The BET surface area and pore volume of mpg-C_3N_4 are 189.78 m^2/g and 0.65 cm^3/g, respectively, far beyond those of nonmesoporous g-C_3N_4, which are 13.57 m^2/g and 0.27 cm^3/g, respectively. The adsorption amount increases by 2 times for MC-LR and 1.2 times for MC-RR with the increasing of surface area and pore volume. Therefore, the adsorbents with larger surface area and pore volume manifest higher adsorption capacities of MCs molecules than those with low ones.

Furthermore, we can obtain from Fig. S4 that the zeta potential of materials (0.15 mg /mL) increase from —22.21 mV to +17.07 mV after protonation at pH 7.0. Corresponding, the adsorption equilibrium time decrease from about 100 min to 30 min (Fig. 5), the adsorption amount of MCs leveled up to about 485.0 μg/g, revealing that the protonation process greatly enhance the uptake efficiency of MCs onto the adsorbent and it also demonstrates electrostatic interaction play an important role in adsorption of MCs on adsorbent.

3.3. Kinetics for the adsorption

The time-dependent adsorption capacity is obtained to study the kinetics for the adsorption of MCs on mpg-C_3N_4-H^+ (Fig. 6 a, b). It is observed that the removal of MCs from aqueous is associated with an extremely rapid initial stage and the adsorption reaches equilibrium is achieved within 15 min for both MC-LR/RR at 50.0 μg/L. The equilibrium adsorption capacity increased from 474.9 to 1483.6 μg/g for MC-LR and 481.4 to 1949.0 μg/g for MC-RR as initial concentration varied from 50.0 to 200.0 μg/L. Furthermore, the adsorption capacity significantly increased as the initial concentration of MCs increased, indicating

Table 1. Kinetic parameters for the adsorption of MCs on mpg-C_3N_4-H^+ at 30 ºC.

			Pseudo-second-order kinetic model			Intraparticle diffusion model		
	C_0/(ppb)	$q_{e(exp)}$/(μg/g)	$q_{e(cal)}$/(μg/g)	k_2/(μg/g min)	R^2	K_{id}/(μg/g $min^{1/2}$)	C/(μg/g)	R^2
MC-LR	50.0	474.87	476.19	1.04E-03	1.0000	15.41	372.52	0.5796
	100.0	803.59	806.45	3.82E-04	1.0000	63.23	427.36	0.5664
	200.0	1483.61	1484.42	2.99E-04	1.0000	144.19	663.01	0.9986
MC-RR	50.0	481.44	480.77	3.01E-02	1.0000	0.06	479.56	0.4393
	100.0	967.69	970.87	4.74E-04	1.0000	126.97	239.53	0.9842
	200.0	1949.04	1956.97	1.13E-04	1.0000	189.22	501.67	0.9885

the favorable adsorption at high concentrations of MCs.

Three of the most widely used kinetic models, i.e. Pseudo-second-order equation, Pseudo-first-order equation and intra-particle diffusion model were used to examine the adsorption kinetic behavior of MCs onto mpg-C_3N_4-H^+. The best-fit model is selected based on the linear regression correlation coefficient values (R^2). The result is showed in table 1.

Pseudo-first-order kinetic model might be represented by Eq(1).

$$\ln(q_e - q_t) = \ln q_e - k_1 t \quad (1)$$

Where k_1: the apparent pseudo-first-order constant (min^{-1}); q_e: amount adsorbed at equilibrium (μg/g); q_t: amount adsorbed at time t (μg/g); t: adsorption time (min). Therefore, the first order kinetic constant (k_1) can be calculated by k_1= −slope when the ln (q_e−q_t) is plotted against t.

The adsorption data were also analyzed using the versatile pseudo-second-order kinetic model:

$$\frac{t}{q_t} = \frac{1}{(k_2 * q_e^{\,2})} + \frac{t}{q_e} \quad (2)$$

Where k_2: the apparent pseudo-second-order rate constant (g/μg/min) Similarly, the second-order kinetic constant (k_2) can be calculated by the values of $1/q_e$ and $1/k_2q_e^2$ when the t/q_t is plotted against t.

An intra-particle mass transfer diffusion model proposed by Weber and Morris can be written as follows:

$$q_t = K_{id} T^{1/2} + C \quad (3)$$

Where q_t (mg /g) is the adsorption capacity at time t, K_{id} (μg/g $min^{1/2}$) the intraparticle diffusion rate constant, and C the intercept. The K_{id} value can be found from the slope of q_t against $t^{1/2}$ plot.

The pseudo-first-order kinetic model data was showed in Supplementary data table.1. Obviously the correlation coefficient values was so low that pseudo-first-order kinetic model was not suitable be chosen to describe the adsorption. All the experimental data showed better compliance with pseudo-second-order kinetic model in terms of higher correlation coefficient values (R^2 > 0.9999) and closer values between $q_{e,cal}$ and $q_{e,exp}$ (Fig. 6c, d). It is clear that the adsorption of MCs on the adsorbent is well described by a versatile pseudo-second-order kinetic model which is based on the adsorption capacity on the solid phase. Moreover, the rate constant k_2 decreased as the initial MCs concentration increased, indicating that the rate-limiting step might be chemical adsorption, involving valency forces through sharing or exchange of electrons between anions and the Adsorbent while chemisorption is a kind of adsorption which involves a chemical reaction between the adsorbant surface and the adsorbate.[33] Besides, the possibility to establish π–π interaction between the benzene rings in MCs and mpg-C_3N_4-H^+ also play important roles.

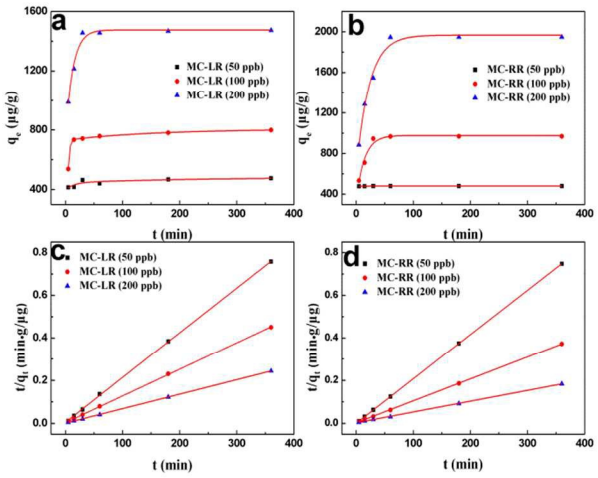

Fig. 6 (a) (b) Effect of contact time on the adsorption of MCs on mpg-C_3N_4-H^+ (0.1 mg) at different initial concentrations of MCs at 30 ºC; pH 7.0; and (c) (d) plots of pseudo-second-order kinetics for the adsorption of MCs on mpg-C_3N_4-H^+ (0.1 mg).

Table 2. Isotherm model constants and regression coefficients for MCs adsorption onto mpg-C_3N_4-H^+.

		Langmuir isotherm constants			Freundlich isotherm constants		
	T(K)	q_m/(μg/g)	K_L/(L/μg)	R^2	$1/n$	K_F/(μg/g(L/μg)$^{1/n}$)	R^2
MC-LR	293.0	2360.96	0.05	0.9980	0.59	140.89	0.9697
	303.0	2320.19	0.05	0.9986	0.62	104.56	0.9663
	313.0	2315.47	0.04	0.9962	0.56	185.94	0.9493
	323.0	2249.75	0.03	0.9988	0.57	163.89	0.9529
MC-RR	293.0	2868.78	0.08	0.9988	0.60	253.64	0.9453
	303.0	2685.65	0.07	0.9978	0.58	231.59	0.9493
	313.0	2534.80	0.06	0.9968	0.57	205.55	0.9589
	323.0	2360.56	0.05	0.9946	0.56	186.29	0.9586

For intra-particle mass transfer diffusion model, If the value of C is zero, then the rate of adsorption is controlled solely by intraparticle diffusion for the entire adsorption period.[34] However all the linear portions don't pass through the origin (Supplementary data Fig. S6) and the plot of q_t versus $t^{1/2}$ shows multilinear portions, suggesting that more than one process affect the adsorption. All the intercept of plots reflected obvious boundary layer effect (Table 1), revealing that film (boundarylayer) diffusion controlled the adsorption rate at the beginning,[35] but intra-particle diffusion is not solely rate-controlling step, for the larger intercept, the greater the contribution of the surface adsorption in the rate controlling step.

3.4. Isotherm modelling

The adsorption isotherms of MCs on mpg-C_3N_4-H^+ were measured at four different temperatures (Supplementary data Fig. S7.). In order to describe the adsorption isotherm more scientifically, the Langmuir and Freundlich model are selected for this study. The linearized Langmuir isotherm equation (5) and Freundlich isotherm equation (6) can be expressed as follows:

$$\frac{C_e}{q_e} = \frac{C_e}{q_m} + \frac{1}{q_m b} \quad (5)$$

$$q_e = K_F C_e^{1/n} \quad (6)$$

Where C_e: equilibrium concentration of adsorbate (μg/L); q_e: amount adsorbed at equilibrium (μg/g); q_m: maximum adsorption capacity (μg/g); b: Langmuir constant (L/μg or L/mol); K_F: the Freundlich adsorption constant (μg/g(L/μg)$^{1/n}$); $1/n$: another constant related to the surface heterogeneity (unitless). The slope and intercept of linear plots of C_e/q_e against C_e yield the values of $1/q_m$ and $1/q_m b$ for Eq. (5) and the slope and intercept of linear plots of ln q_e against ln C_e yield the values of $1/n$ and ln K_F for equation (6).

The theoretical parameters of adsorption isotherms along with regression coefficients (R^2) are summarized in Table 2. R^2 values of Langmuir model are higher than Freundlich model shows the Langmuir model reasonably a better fit with adsorption process. It is clear that the correlation coefficients for MCs are high and the isotherms are linear over the whole, indicating that the MCs adsorbed on the surface of adsorbent is monolayer coverage. It is notable that an increase in temperature resulted in a corresponding decrease in adsorption capacity of MCs, which showed that uptake of MCs onto mpg-C_3N_4-H^+ is an exothermic process. The mpg-C_3N_4-H^+ showed a very high adsorption capacity of 2360.96 and 2868.78 μg/g from the Langmuir model for MC-LR and MC-RR, respectively while the maximum adsorption capacity obtained with the commercial activated carbon is 1481.7 μg/g and 1034.1 μg/g for MC-LR and MC-RR, respectively.[36]

3.5. Thermodynamics for the adsorption

In the process of MCs adsorption, according to the adsorption equilibrium at different temperatures, the thermodynamic parameters, standard free energy change (ΔG^0, kJ/mol), entropy change (ΔS^0, J/mol/K) and enthalpy change (ΔH^0,kJ/mol), entropy change (ΔS^0, J/mol/K) and enthalpy change (ΔH^0, kJ/mol) can be estimated from the following relationship (Supplementary data Fig. S8.):

$$\Delta G = RT \ln b \quad (7)$$

$$\ln b = \frac{\Delta S}{R} - \frac{\Delta H}{RT} \quad (8)$$

Table 3. Thermodynamic parameters for adsorption

		Thermodynamic parameters		
	T/(K)	ΔG^0/(kJ/mol)	ΔH^0/(KJ/mol)	ΔS^0/(J/mol K)
MC-LR	293.0	-12.49	-21.28	-29.58
	303.0	-12.42		
	313.0	-12.24		
	323.0	-11.53		
MC-RR	293.0	-13.64	-12.56	3.78
	303.0	-13.77		
	313.0	-13.73		
	323.0	-13.77		

(Where R is gas constant)

The Langmuir constant b (dimension: L/mol) can be obtained from the slope/intercept of the Langmuir plot. The enthalpy change ΔH for MCs adsorption over mpg-C_3N_4-H^+ were both negative, -21.28 kJ/mol for MC-LR and -12.56 kJ/mol for MC-RR, respectively, confirming endothermic adsorption in accordance with the decreasing adsorption capacity associated with increasing adsorption temperature. This result may be attributed to high temperature will block the interaction between MCs and adsorbent. The entropy change ΔS were -29.58 J/mol K and 3.78 J/mol K for MC-LR and MC-RR, respectively. The positive ΔS means the increased randomness with adsorption of MC-RR probably because the number of desorbed water molecules is larger than that of the adsorbed MC-RR molecules. On the contrary, the negative ΔS for MC-LR means decreased randomness with adsorption. According to eqn (8), free energies of adsorption at 20 ºC, 30 ºC, 40 ºC and 50 ºC were –12.49, –12.42, –12.24, –11.53 kJ/mol for MC-LR and –13.64, –13.77, –13.73, –13.77 kJ/mol for MC-RR, respectively (Table 3). These negative free energies confirmed that adsorption is spontaneous under the experimental conditions uesd.

3.6. Desorption and regeneration

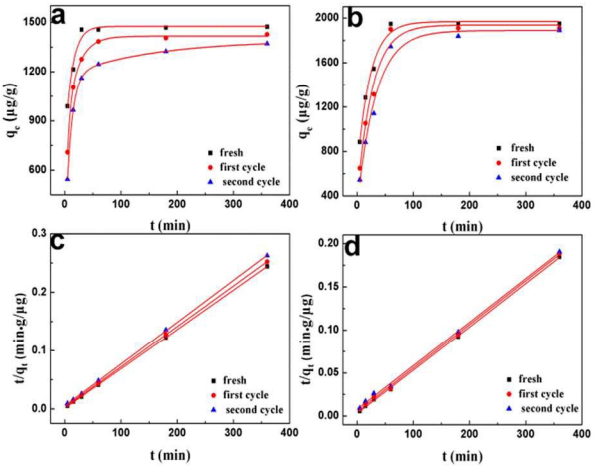

Fig. 7. (a) Effect of contact time on the MC-LR (200.0 μg/L) adsorption at 30 ºC; pH 7.0; (b) Effect of contact time on the MC-RR (200.0 μg/L) adsorption at 30 ºC; pH 7.0; (c)(d) Pseudo-second-order plots to show the re-usability of the mpg-C_3N_4-H^+ in adsorption of MC-LR/ RR.

To evaluate the possibility of regeneration and reusability of mpg-C_3N_4-H^+ as an adsorbent, desorption experiments are conducted. Desorption and regeneration experiments were achieved by using ethanol under ultrasound assisted desorption for 15 min, the effect of two consecutive adsorption–desorption

cycles is studied (Fig.7). The MCs removal efficiency almost keeps a steady value and it is still above 90% after recycling 2 times. These results demonstrate that the mpg-C_3N_4-H^+ can be regenerated and is suitable for adsorptive MCs removal.

FT-IR and SEM of the recycled mpg-C_3N_4-H^+ are characterized and shown in Fig.S2, S5, respectively. From Fig. S2, it can be seen that the characteristic peaks of recycled mpg-C_3N_4-H^+ are very close to original mpg-C_3N_4-H^+, which further confirms that the core chemical skeleton of mpg-C_3N_4-H^+ has remained unchanged after exposed to MCs. Based on Fig. S5, it can also be observed that the the typical slate-like structure are still remain in mpg-C_3N_4-H^+. All these can help to draw the conclusion that the structure of the mpg-C_3N_4-H^+ stable during the adsorption process.

4. Conclusion

In this work, we reported the adsorption of MCs on a highly protonated mesoporous graphitic carbon nitride in view of the adsorption kinetics, isotherm, thermodynamics and regeneration of the sorbent. The measurements indicated that the mpg-C_3N_4 could be protonated by a convenient modification route. It is found that the removal efficiency of MCs through mpg-C_3N_4-H^+ is much better than mpg-C_3N_4 and g-C_3N_4. The results also confirm that mpg-C_3N_4-H^+ can be used in place of activated carbon since it is higher adsorption capacity and more efficient in removing MCs. The good results demonstrated the potential of mpg-C_3N_4-H^+ in adsorption and removal of MCs from aqueous solution.

Acknowledgements

The authors are grateful for the National Nature Sciences Foundation of China (21275029, 201405018), the National Basic Research Program of China (No.2010CB732403), the "12th Five-Year National Science and Technology Support Program" (2012BAD29B06), the Program for Changjiang Scholars and Innovative Research Team in University (No. IRT1116).

References

1. K. P. Loh, Q. Bao, G. Eda and M. Chhowalla, *Nature chemistry*, 2010, 2, 1015-1024.
2. L. Feng, L. Wu and X. Qu, *Advanced Materials*, 2013, 25, 168-186.
3. S. Yang, Y. Gong, J. Zhang, L. Zhan, L. Ma, Z. Fang, R. Vajtai, X. Wang and P. M. Ajayan, *Advanced Materials*, 2013, 25, 2452-2456.
4. Y. Zhang and M. Antonietti, *Chemistry, an Asian journal*, 2010, 5, 1307.
5. M. Groenewolt and M. Antonietti, *Advanced materials*, 2005, 17, 1789-1792.
6. X. Wang, K. Maeda, A. Thomas, K. Takanabe, G. Xin, J. M. Carlsson, K. Domen and M. Antonietti, *Nature Materials*, 2008, 8, 76-80.
7. X. Wang, X. Chen, A. Thomas, X. Fu and M. Antonietti, *Advanced Materials*, 2009, 21, 1609-1612.
8. C. Cheng, Y. Huang, J. Wang, B. Zheng, H. Yuan and D. Xiao, *Analytical chemistry*, 2013, 85, 2601-2605.
9. L.-S. Lin, Z.-X. Cong, J. Li, K.-M. Ke, S.-S. Guo, H.-H. Yang and G.-N. Chen, *Journal of Materials Chemistry B*, 2014, 2, 1031-1037.
10. X. Zhang, H. Wang, H. Wang, Q. Zhang, J. Xie, Y. Tian, J. Wang and Y. Xie, *Advanced Materials*, 2014, 26, 4438-4443.
11. X. Wang, K. Maeda, X. Chen, K. Takanabe, K. Domen, Y. Hou, X. Fu and M. Antonietti, *Journal of the American Chemical Society*, 2009, 131, 1680-1681.
12. K. Takanabe, K. Kamata, X. Wang, M. Antonietti, J. Kubota and K. Domen, *Physical Chemistry Chemical Physics*, 2010, 12, 13020-13025.
13. F. Su, M. Antonietti and X. Wang, *Catal. Sci. Technol.*, 2012, 2, 1005-1009.
14. S. Ramesh, L. M. Ericson, V. A. Davis, R. K. Saini, C. Kittrell, M. Pasquali, W. Billups, W. W. Adams, R. H. Hauge and R. E. Smalley, *The Journal of Physical Chemistry B*, 2004, 108, 8794-8798.
15. Y. Zhang, A. Thomas, M. Antonietti and X. Wang, *Journal of the American Chemical Society*, 2008, 131, 50-51.
16. P. Shen, Q. Shi, Z. Hua, F. Kong, Z. Wang, S. Zhuang and D. Chen, *Environment International*, 2003, 29, 641-647.
17. I. R. Falconer, *Environmental Toxicology*, 1999, 14, 5-12.
18. T. Jurczak, M. Tarczynska, K. Izydorczyk, J. Mankiewicz, M. Zalewski and J. Meriluoto, *Water Research*, 2005, 39, 2394-2406.
19. S. Merel, B. LeBot, M. Clément, R. Seux and O. Thomas, *Chemosphere*, 2009, 74, 832-839.
20. D. G. Bourne, R. L. Blakeley, P. Riddles and G. J. Jones, *Water Research*, 2006, 40, 1294-1302.
21. C. Svrcek and D. W. Smith, *Journal of Environmental Engineering and Science*, 2004, 3, 155-185.
22. R. J. Morris, D. E. Williams, H. A. Luu, C. F. Holmes, R. J. Andersen and S. E. Calvert, *Toxicon*, 2000, 38, 303-308.
23. M. Sathishkumar, S. Pavagadhi, K. Vijayaraghavan, R. Balasubramanian and S. Ong, *Journal of hazardous materials*, 2010, 184, 417-424.
24. H. Yan, A. Gong, H. He, J. Zhou, Y. Wei and L. Lv, *Chemosphere*, 2006, 62, 142-148.
25. S. Pavagadhi, A. L. L. Tang, M. Sathishkumar, K. P. Loh and R. Balasubramanian, *Water Res*, 2013, 47, 4621-4629.
26. W. Teng, Z. Wu, D. Feng, J. Fan, J. Wang, H. Wei, M. Song and D. Zhao, *Environmental science & technology*, 2013, 47, 8633-8641.
27. W. Teng, Z. Wu, J. Fan, H. Chen, D. Feng, Y. Lv, J. Wang, A. M. Asiri and D. Zhao, *Energy & Environmental Science*, 2013, 6, 2765-2776.
28. W. Xia, X. Zhang, L. Xu, Y. Wang, J. Lin and R. Zou, *RSC Advances*, 2013, 3, 11007-11013.
29. Y. Zhao, D. Yu, H. Zhou, Y. Tian and O. Yanagisawa, *Journal of materials science*, 2005, 40, 2645-2647.
30. X. Li, J. Zhang, L. Shen, Y. Ma, W. Lei, Q. Cui and G. Zou, *Applied Physics A*, 2009, 94, 387-392.
31. P. De Maagd, A. J. Hendriks, W. Seinen and D. T. Sijm, *Water Research*, 1999, 33, 677-680.
32. X. Wu, B. Xiao, R. Li, C. Wang, J. Huang and Z. Wang, *Environmental science & technology*, 2011, 45, 2641-2647.
33. G. Crini, H. N. Peindy, F. Gimbert and C. Robert, *Separation and Purification Technology*, 2007, 53, 97-110.
34. V. Vadivelan and K. V. Kumar, *Journal of Colloid and Interface Science*, 2005, 286, 90-100.
35. L. Wang, J. Zhang, R. Zhao, C. Li, Y. Li and C. Zhang, *Desalination*, 2010, 254, 68-74.
36. S. Pavagadhi, A. L. Tang, M. Sathishkumar, K. P. Loh and R. Balasubramanian, *Water Res*, 2013, 47, 4621-4629.